Factors Controlling Hole Injection in Single Conjugated Polymer Molecules†

Leonid Fradkin, Rodrigo E. Palacios, Joshua C. Bolinger, Kwang-Jik Lee, William M. Lackowski, and Paul F. Barbara*

Center for Nano and Molecular Science and Technology, University of Texas, Austin, Texas 78712

Received: January 19, 2009; Revised Manuscript Received: February 2, 2009

New insights on the molecular level details of the recently reported light-assisted injection of positive charge into single conjugated polymer chains are reported. Extensive new fluorescence−voltage single molecule spectroscopy (FV-SMS) measurements were performed on single chains of the archetypical conjugated polymer MEH-PPV embedded in a capacitor device to complement previous studies of the influence of the bias scan rate and optical excitation intensity. The use of a vacuum microscope allowed for the precise control of the device atmosphere, demonstrating the influence of triplet states in the MEH-PPV on the FV-SMS modulation. For identical device conditions, little variation was observed in the rate and yield of charging from molecule to molecule. Through the use of thicker supporting matrices and insulating polymer "blocking layers", it was determined that good electrical contact between the hole transport layers and the single molecules was necessary for charge injection. The results demonstrate the complexity of charge transfer processes at the interface of organic semiconductors and highlight the ability of single molecule methods to advance the understanding of such processes at the nanoscale.

1. Introduction

The transfer of positive charge (holes) across an organic heterojunction is a central process in organic light emitting diodes (OLEDs)[1−4] and other organic electronic devices.[5−8] We recently reported that hole transfer (i.e., injection) from a hole-transport-layer (HTL) into single conjugated polymer chains can be rapidly accelerated by optically exciting the polymer molecule, and ultimately forming deeply trapped positive charges, i.e., holes.[9−11] This light-assisted injection of positive charge carriers (holes) was assigned to a light-induced hole-transfer mechanism (denoted by LIHT) in which excitons in the polymer chain interact across the polymer/HTL interface with holes that accumulate in the HTL under suitable bias.[2,12] The formation of deeply trapped holes (DTH) at interfaces in organic semiconductor bulk heterojunctions[2,13−22] has been observed in various contexts and is apparently due to chemical rearrangement/modification of the charged form of the specific materials.[13,15,17,20−24] DTH may be responsible for hysteresis that is commonly observed in the current (*i*) vs. voltage (*V*) curves for various types of organic electronics (also known as the bias stress effect), which is due apparently to the creation and interfacial buildup of DTH.[14,15,23−26]

In this paper, we explore the kinetics of MEH-PPV single-molecule charging in considerably more detail than previously described to obtain new insights on the molecular level details of the light-induced hole-transfer (LIHT) process. As in previous papers, we employ photoinduced hole injection to investigate charge transfer across heterojunctions into single-polymer chains, using a device geometry in which holes are injected into single-molecule capacitors of the conjugated polymer poly(2-methoxy-5-(2′-ethylhexyloxy)-1,4-phenylenevinylene) (MEH-PPV). The specific hole-injection process that was investigated involves hole transfer from a carbazole derivative (4,4′-*N*,*N*′-dicarbazolebiphenyl, CBP) to a MEH-PPV single-polymer chain at a CBP/MEH-PPV interface.[10,11] Since direct electrical measurements of the small number (∼1−5) of charges injected per single molecule is exceedingly difficult, we employ an indirect single-molecule fluorescence approach in which the amount and rate of hole injection from the HTL into individual, isolated polymer chains was monitored with fluorescence quenching as a measure of the charge density in each polymer chain. This approach is a convenient means for exploring the barriers and rates of hole injection in semiconductor nanodomains.

We investigate the single-molecule fluorescence vs. voltage (FV-SMS) behavior with a triangular bias waveform for large ensembles of MEH-PPV single-polymer chains located at a CBP interface in a capacitor device geometry (type A) that is shown in Figure 1. In this approach, at positive bias (see Figure 1 for the sign convention), holes are transferred from the gold electrode through an intermediate HTL material, *N*,*N*′-bis(3-methylphenyl)-*N*,*N*′-diphenylbenzidene (TPD), and then to CBP to produce a hole space charge on the CBP side of the CBP/MEH-PPV interface. In contrast, at negative bias, the device is free of a significant amount of space charge at equilibrium. Using FV-SMS we investigate the kinetics of charge injection into MEH-PPV as a function of bias scan rate, optical excitation intensity, atmosphere (O_2 vs. no O_2), and in the presence or absence of a charge blocking layer (type B, Figure 1). One topic we address is whether singlet excitons or triplet excitons are the main source of injection for the LIHT process. We also examine to what extent energetic vs. thermodynamic processes are reflected in the shape of the fluorescence−voltage (F−V) quenching curves. Finally, we explore how the charge injection process depends on electrical contact between the single MEH-PPV chains and the CBP HTL.

2. Experimental Section

Samples consisting of large area, multilayered devices, as shown in Figure 1 were fabricated by methods that have been described in detail elsewhere.[9] Briefly, SiO_2 was grown as an

† Part of the "George C. Schatz Festschrift".

* To whom correspondence should be addressed. E-mail: p.barbara@mail.utexas.edu.

10.1021/jp900562w CCC: $40.75
Published on Web 03/04/2009

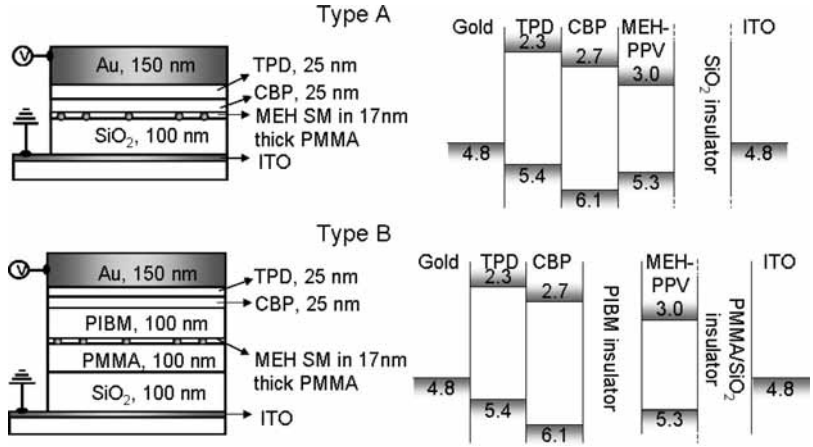

Figure 1. Hole-injection device structure and corresponding energy band diagram of two types of devices, type A and type B. Type B device includes a blocking polymer layer (PIBM) sandwiched between the hole-injection layers of TPD and CBP and the single molecules of MEH-PPV. Layer thicknesses for the devices used in this study are shown above unless noted otherwise.

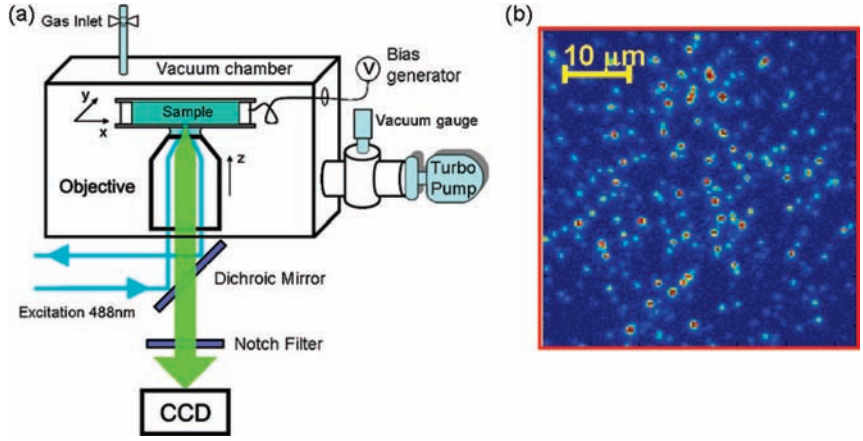

Figure 2. (a) Schematic of the home-built wide field vacuum microscope. (b) Representative image of single molecules of MEH-PPV in the device structure shown in Figure 1.

insulating layer on a patterned ITO coverslip (Evaporated Coatings, etc.) via a low-temperature, inductively coupled plasma-assisted chemical vapor deposition method with a resulting thickness of 100 nm. The layer of single-molecule MEH-PPV (Uniax, $M_w = 1000$ kg/mol) was spin casted from toluene (Sigma Aldrich, anhydrous 99.8%) with a supporting matrix of poly(methyl methacrylate) (PMMA) (Sigma Aldrich, $M_w = 101$ kg/mol) to prevent aggregation. For type B devices, an isolating layer of poly(isobutyl methacrylate) (PIBM) (Acros, $M_w = 300$ kg/mol) was spun from the orthogonal solvent cyclohexane. Hole transport layers of 4,4′-*N*,*N*′-dicarbazolebiphenyl (CBP) (Sigma Aldrich, 98%) and *N*,*N*′-bis(3-methylphenyl)-*N*,*N*′-diphenylbenzidene (TPD) (Sigma Aldrich, 99%) were deposited by thermal evaporation under vacuum (10^{-6} Torr) at a rate of 1−2 Å/s for a thickness of 25 nm for each layer. The top Au electrode was deposited by thermal evaporation with a thickness of 150 nm (8 nm for the experiments of triplet vs singlet exciton charge injection). Patterning of the HTLs and top electrode was accomplished through the use of shadow masks, resulting in four independent devices per coverslip/sample. All fabrication was performed in a glovebox (O_2 and H_2O concentrations below 5 ppm) except for the SiO_2 deposition where exposure to atmosphere was necessary. Devices were wired inside the glovebox by using silver paint and transferred via an airtight container. The vacuum chamber was prefilled with high-purity argon (Matheson Trigas) or N_2 (Praxair) to minimize the sample exposure to the laboratory atmosphere.

The experimental apparatus is a home-built wide field vacuum microscope (Figure 2a). A small, ∼4 L vacuum chamber is equipped with a mechanical rotary pump coupled to a turbomolecular pump and is capable of reaching a base pressure of 10^{-7} Torr. A combination of vacuum gauges (InstruTech IMG-410 and CMV-221) were used to monitor the pressure inside the chamber. When the effects of atmosphere on the quenching dynamics were studied, prefilled flasks of ultrahigh-purity gas, N_2 (Praxair, 99.995%) or O_2 (Air Liquide, 99.995%), were coupled into the vacuum chamber in a controlled manner.

All optics are located outside of the chamber with the exception of the long working distance microscope objective (Zeiss LD Achroplan 40×/0.6NA Corr). A quartz view port window couples the excitation and fluorescence into and out of the chamber. Fluorescence excitation is provided by the 488-nm line of a multiline Ar ion laser (Melles Griot, 543 series). The laser line is spatially dispersed by using a prism and further spectrally isolated with a 488-nm interference filter (Chroma). Laser intensity is attenuated with neutral density filters to intensities appropriate for single-molecule spectroscopy. Fluorescence intensity is collected and stray excitation light is rejected with a dichroic mirror (Chroma, Z488RCD) and a holographic notch filter (Kaiser, SuperNotch-Plus, 488 nm).

Wide-field fluorescence images were acquired with an electron multiplying CCD detector array (Andor, iXon-DU-897), using the commercially available program Metamorph (Molecular Devices, 1992−2007, Version 7.1.0.0). The image acquisi-

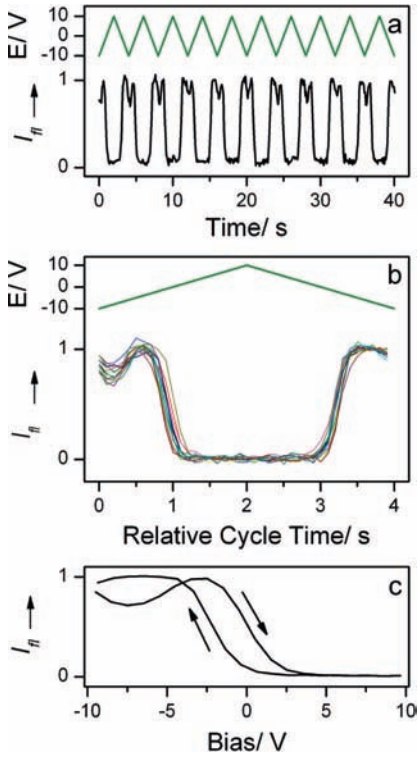

Figure 3. (a) Ensemble average of 150 single-molecule normalized fluorescence-intensity transients. The bias modulation function is presented at the top of the panel (green). (b) Normalized single-molecule fluorescence-intensity transients. Each transient represents the single-molecule response to the applied bias and synchronously averaged over 23 bias cycles. The bias period is shown by the green line. (c) Ensemble average of 150 single-molecule F−V trajectories. Arrows indicate the direction of the bias scan.

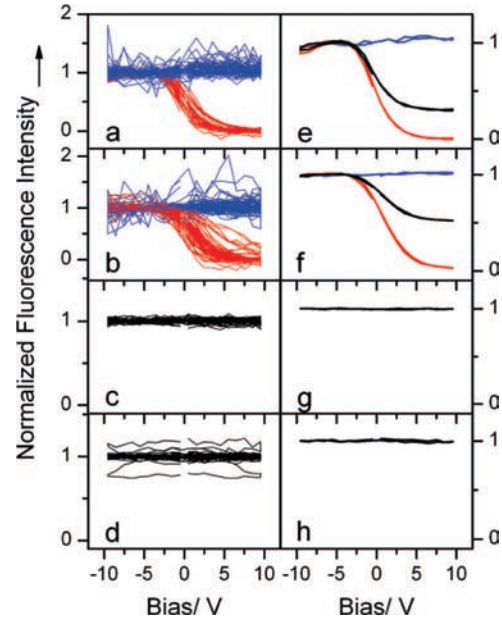

Figure 4. (a-d) F−V transients of single-molecule MEH-PPV in hole-injection devices with different geometries. (a) Type A device with a 100-nm-thick PMMA supporting matrix layer. (b) Type A device with a 200-nm-thick PMMA supporting matrix layer. Blue transients represent molecules that showed no fluorescence modulation. Red transients represent molecules that showed fluorescence modulation with applied bias. (c) Type B device with dimensions as shown in Figure 1, with a PIBM isolating layer placed between the single-molecule MEH-PPV and the HTLs. (d) Type A device with 25-nm-thick PMMA supporting matrix, with the CBP and TPD HTLs omitted. (e−h) Ensemble averages of the individual transients shown in panels a−d. Black traces corresponding to the ensembles shown in panels e and f represent all molecule transients while the red and blue traces represent only the fluorescence modulating and nonmodulating molecules, respectively.

tion was synchronized to a time varying bias applied to the sample by a programmable function generator (Wavetek, 29A). A home-written Matlab routine was used to find the individual bright spots (due to the single molecules) in the CCD images and to calculate the integrated fluorescence intensities of the spots. The time dependence of the fluorescence of individual spots was determined from a set of acquired images and it was ensemble averaged and/or synchronously averaged over several bias cycles as needed.

3. Results and Discussion

Basic Experiment. Before describing the new results, we briefly review the basic FV-SMS experiment. As shown in Figure 2b, the fluorescence image exhibits spots due to individual, isolated single molecules of MEH-PPV imbedded in a type A device (see Figure 1). This particular image was recorded in the vacuum microscope described in the Experimental Section and shown schematically in Figure 2a. The use of the vacuum microscope allows for control of the dissolved gases and moisture in the devices. Figure 3a portrays FV-SMS ensemble data (average of hundreds of individual polymer chains) for several bias cycles of the applied triangular potential. The time-varying intensity reveals a dramatic decrease during periods of positive bias due to fluorescence quenching from hole injection into MEH-PPV single polymer chains from the CBP HTL. Holes are transferred from the Au electrode through the TPD and CBP HTLs into the MEH-PPV single-polymer chains. The intensity vs. time curves from cycle to cycle are highly reproducible allowing reliable synchronous averaging, resulting in the intensity vs. time curves shown in Figure 3b. However, below we show that the intensity vs. time curves for type A devices do vary over the time period of the first <10 cycles due to a relaxation phenomena. In those cases, the synchronous averaging of the FV-SMS data was started after 10 cycles to ensure that the average reflects the steady-state response. The synchronous averaged FV-SMS data in Figure 3c show the expected quenching at positive bias due to hole-injection.

Control of the Electrical Contact between MEH-PPV and the CBP HTL. Figure 4 shows the effect of sample preparation conditions on the MEH-PPV polymer chain quenching. Panels a and b of Figure 4 show a complete ensemble of synchronously averaged FV-SMS curves for individual transients for type A devices with 100- and 200-nm-thick MEH-PPV/PMMA layers in place of the 17-nm layer as shown in Figure 1 (type A). The individual curves are well sorted into two types, i.e., non-quenching (blue curves) and quenching (red curves). The sorting criterion is an intensity threshold of 50% at a bias of 10 V. We assign the red curves to molecules that are in close contact with the CBP HTL while the blue curves are assigned to molecules that are too far away to be able to transfer charge with the HTL. This behavior was reproduced for different devices and the same type of substrate and for many fabrication runs over a year duration using different batches of substrates, SiO_2 runs, etc. Interestingly, for devices with the 17-nm support matrix layers (as shown in Figure 1), more than 95% and sometime 100% of the molecules exhibit highly analogous quenching curves. Thus, for the 17-nm devices, most of the MEH-PPV molecules are in excellent contact with the CBP HTL layer.

Further support for the necessity for electrical contact between the MEH-PPV and CBP layers to achieve hole-injection and hole-induced quenching is found in the FV-SMS data for the type B device as shown in Figure 4c, which contains a PIBM isolating layer placed between the single MEH-PPV molecules and the carbazole HTL. Over 98% of the single molecules show no modulation with applied bias. It is interesting to consider the FV-SMS data for a device where the HTL layers are completely removed, as shown in Figure 4d. For this device, we observe a decrease in the number of bright fluorescence spots in the wide-field fluorescence images when the gold layer is added on top of the MEH-PPV/PMMA layer. This decrease in the number of fluorescence spots is attributed to fluorescence quenching of the subpopulation of MEH-PPV chains that are in contact with the gold layer due to energy transfer[27,28] rather than hole injection. Presumably, polymer chains that are not in contact with the gold layer are responsible for the bright spots which, as expected, do not undergo significant fluorescence quenching with applied bias.

The right-hand-side column in Figure 4 portrays FV-SMS data that are both synchronously time-averaged and ensemble averaged (for many chains) showing subensembles for quenching (red) and nonquenching (blue) polymer chain, as well as full ensembles (black). One important observation from this high signal-to-noise data is that the blue subensemble shows virtually no dependence on bias even though a relatively mild 50% quenching threshold was employed to sort the data. This demonstrates that the electric field that is present in the PMMA layer in these devices does not induce a significant amount of quenching in the isolated MEH-PPV chains. In addition, field-induced quenching would be expected to exhibit a symmetrical response with respect to bias, at least at the ensemble level. Thus, the absence of polymer chains that show quenching at negative bias also rules out a significant electric field effect on the fluorescence intensity of MEH-PPV in these devices.

Another interesting observation is that the red subensembles (and individual red FV-SMS curves) exhibit essentially 100% quenching. Indeed, for the 17-nm MEH/PMMA layer devices, virtually all the polymer chains show essentially 100% quenching. The black ensemble curves for devices with significant populations of both quenching and nonquenching molecules are misleading when compared to individual chain behavior. This is often the case for the ensemble averaged data for heterogeneous samples.

As stated above, only molecules in close contact with the CBP layer should be able to exhibit hole-induced quenching since hole transfer should only be possible for polymer chains that are within a few angstroms of CBP due to the rapid falloff of charge transfer rates with distance.[29] Thus, for devices with thick supporting matrices, the observation of polymer chains for which the fluorescence is not quenched is not surprising. However, two aspects of the data are surprising. First, the fraction of quenched polymer chains far exceeds that expected from a uniform spatial distribution of polymer chains within the PMMA supporting layer; 70% of molecules show fluorescence quenching in the 100-nm-thick supporting layer while 50% of molecules show fluorescence quenching in the 200-nm-thick layer. Second, the strongly bimodal nature of the observed quenching (red vs. blue) of the set of single molecule curves suggests that there is also a bimodal distribution of MEH-PPV/CBP distances. Both effects can be explained by the hypothesis that most MEH-PPV is directly located on the top surface of the MEH-PPV/PMMA film after it is prepared by spin-coating. This location would allow for direct contact with the CBP layer after it is thermally deposited on top of the MEH-PPV/PMMA film in the fabrication process.

The placement of MEH-PPV on top of the film could be a consequence of a segregation effect during spin-coating in which MEH-PPV, being much more soluble in the spin-coating solvent (toluene) than PMMA, remains in solution longer and thus it is placed on top of the PMMA layer. A similar mechanism has been observed for spin-coating of polystyrene-coated metal nanoparticles with solubilizing groups bound to their surface.[30] It is also possible that the surface energy of MEH-PPV could be lower than that of toluene such that it will segregate to the surface during the spincasting process.

Triplet vs. Singlet Exciton Induced Charge Injection. The relative importance of MEH-PPV singlet excitons vs. triplet excitons in the FV-SMS data was explored by examining the effect of added oxygen. For these measurements, the devices were fabricated with a relatively thin (~8 nm) and porous gold layer to allow for the penetration and removal of gases in the atmosphere into and out of the interior of the devices. The major observed effect of added oxygen on the device is to remove the "fluorescence dip" at negative bias observed in the FV-SMS data. Previous papers from our group have identified this feature with the buildup of triplets in the single-polymer chains as a result of intersystem crossing from singlet excitons.[9] Triplet excitons are themselves fluorescence quenchers, but when the triplet is exposed to holes from the CBP layer, the triplets are removed by a charge transfer mechanism and the quenching due to triplets is removed. (For only slightly positive biases the holes actually return to the CBP layer.) The combined effect of triplets quenching by holes and singlet exciton quenching by triplets produces the fluorescence dip, as described in previous studies from this laboratory.[31,32] An important aspect of this effect is that in single-polymer chains, the triplet population fluctuates primarily between zero and one triplet per chain. When a second triplet is added to a chain that already contains one triplet exciton, a rapid annihilation event occurs that removes both triplets effectively limiting the depth of the fluorescence quenching due to triplets observed at negative bias.

As shown in Figure 5 when oxygen is added to the device, the fluorescence-dip is removed due presumably to the rapid quenching of triplets by oxygen.[32] This ensures that the triplet population never gets large enough to produce singlet quenching by triplets and, in turn, the fluorescence-dip effect. The observation that the dip effect reappears when oxygen is removed by either evacuating the sample or flushing the chamber with ultrapure nitrogen is further evidence in support of the role of triplet quenching in producing the fluorescence-dip. It should be emphasized that the charge-induced quenching at the higher biases of these experiments is probably due to the buildup of holes in the MEH-PPV material not just the quenching of singlet excitons by the proximity of CBP holes. In this regard it is interesting to explore which type of MEH-PPV exciton (triplet or singlet) is responsible for the hole-injection process.

The observation that the positive bias region of the FV-SMS curves is not significantly impacted by the addition or removal of oxygen strongly suggests that singlet excitons are capable of inducing hole injection and subsequent quenching. However, there are small differences in the curves with and without oxygen which might indicate that triplets can induce hole injection in addition to singlet excitons. There are additional uncertainties in the FV-SMS curves from device to device and run to run which are probably due to charge trapping at poorly understood interfaces in the devices causing small shifts in the voltages where charging and discharging occurs. These shifts tend to

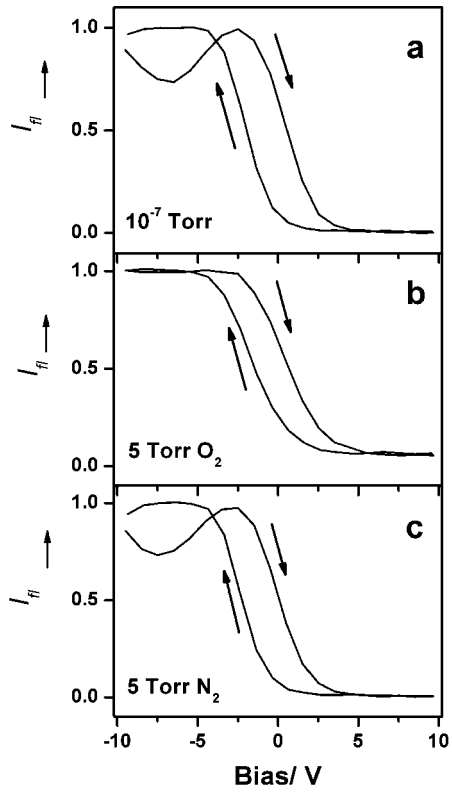

Figure 5. Ensemble average fluorescence−voltage trajectories of 60 molecules taken at different environmental conditions: (a) at a vacuum of 10^{-7} Torr; (b) in the presence of 5 Torr of ultrapure oxygen; and (c) at 5 Torr of ultra pure nitrogen gas. The excitation power and the bias scan rate were 8.4 W/cm^2 and 10 V/s correspondingly. Arrows indicate the direction of the bias scan.

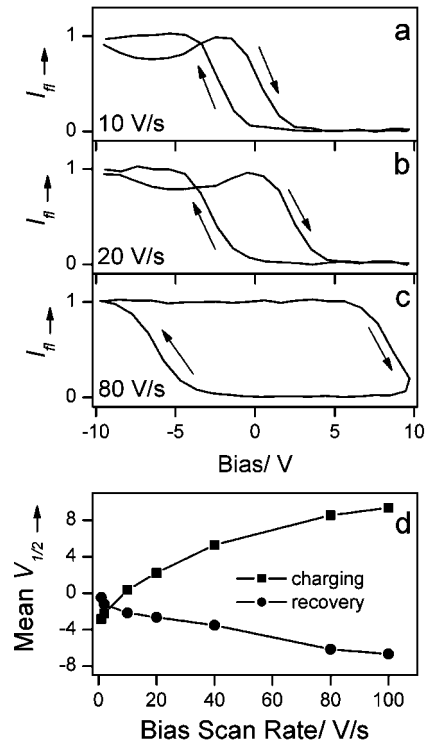

Figure 6. (a−c) Ensemble average of ∼100 single-molecule F−V trajectories measured for a type A device. A triangular bias function, from −10 V to +10 V, was applied across the device. For all panels the excitation intensity was 8.4 W/cm^2 and the bias scan rate is shown for each transient. Arrows indicate the direction of the bias scan. (d) Average $V_{1/2}$ for the quenching and recovery of the fluorescence as a function of the bias scan rate for 100 molecules.

mask subtle changes in the FV-SMS curves and make it difficult to unequivocally explore the role of triplets in the charge injection.

FV-SMS Data vs. Bias Scan Rate and Laser Excitation Power. Generally speaking two main factors contribute to the energetic barrier for hole injection into a conjugated polymer (CP) layer from an adjacent hole-transport layer (HTL): the offset of the energy of the highest occupied molecular orbital of the two materials ($E_{HOMO,CP} - E_{HOMO,HTL}$) and modifications to this energy due to surface dipoles and other effects which can shift the vacuum level energy. Despite the use of a CBP/MEH-PPV heterojunction that would be expected to exhibit energetically favorable thermal hole injection, no injection was observed in the dark under positive bias as described in previous papers.[9−11] This result suggests that the effective E_{HOMO} of single-conjugated polymer chains is actually lower than the bulk material, due perhaps to environmental or conformational effects.

According to the LIHT mechanism, the barrier for hole injection can be overcome through an interaction of CBP holes and MEH-PPV excitons at the CBP/MEH-PPV interface. In addition, electrical modeling shows that the CBP hole concentration increases as the bias on the device increases (in the positive direction). Thus, the rate of hole injection should depend both on the CBP hole concentration (which depends on bias) and the concentration of MEH-PPV excitons (which depends on the excitation light intensity). Figure 6a−c portrays how the FV-SMS data varies as a function of bias scan rate at fixed excitation rate. The observed behavior is highly consistent with a hole-injection process that is sufficiently slow that it cannot "keep up" with the rapid, linearly scanned bias. However, since the hole-injection process is bias dependent, it eventually becomes sufficient to yield 100% quenching. This is summarized in Figure 6d where the mean bias at which the single-chain curves become 50% quenched during the upward scan ($V_{1/2}$ square symbol) and downward scan ($V_{1/2}$ round symbol) is plotted as a function of scan rate. The observation of hysteresis is highly consistent with slow, time-resolvable charging and discharging kinetics.

The first column in Figure 7 portrays how the FV-SMS data vary as the laser excitation intensity is decreased. As expected for the LIHT mechanism, the FV-SMS data show an increase in hysteresis as the laser power is lowered, consistent with a slower hole-injection rate. The hysteresis is especially apparent in the quenching portion of the cycle with the recovery portion unaffected by changes in the light intensity at these powers. The $V_{1/2}$ shifts toward higher bias as the excitation power is decreased. This effect is milder, however, than the effect of scan rate on the hysteresis that was shown in Figure 6. For example, in Figure 6 an increase in scan rate by a factor of 4, from 20 to 80 V/s produced a shift in $V_{1/2}$ of 6 V. In contrast, a decrease of excitation intensity by a factor of more than 10 from 8.4 to 0.65 W/cm^2 only shifts $V_{1/2}$ by 3 V. This demonstrates that there may be more than one factor that controls the threshold for hole injection and the associated hysteresis. It may be that both charging of the CBP layer and hole transfer across the CBP/MEH-PPV interface play a role in the hysteresis.

Another difference between the effect of excitation intensity and bias scan rate is the apparent shift in the $V_{1/2}$ values for discharging. While scanning faster decreases the $V_{1/2}$ value due to hysteresis, reducing the excitation light intensity actually increases $V_{1/2}$. This is especially apparent by examining the histograms of $V_{1/2}$ for charging (blue) and discharging (red) that

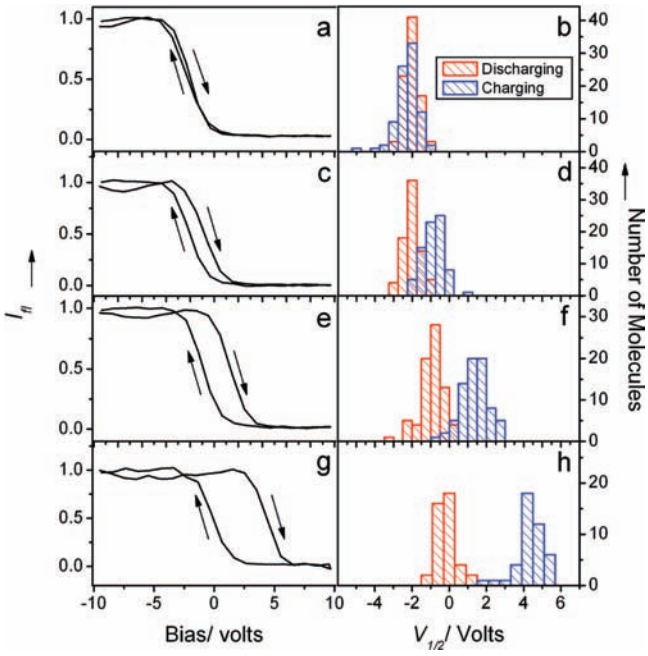

Figure 7. (a, c, e, g) Ensemble average F−V transients measured at 10 V/s bias scan rate and with excitation intensities as follows: (a) 84, (c) 26, (e) 8.4, and (g) 0.65 W/cm^2. (b, d, f, h) Histograms of the $V_{1/2}$ value for the corresponding ensemble average in each row.

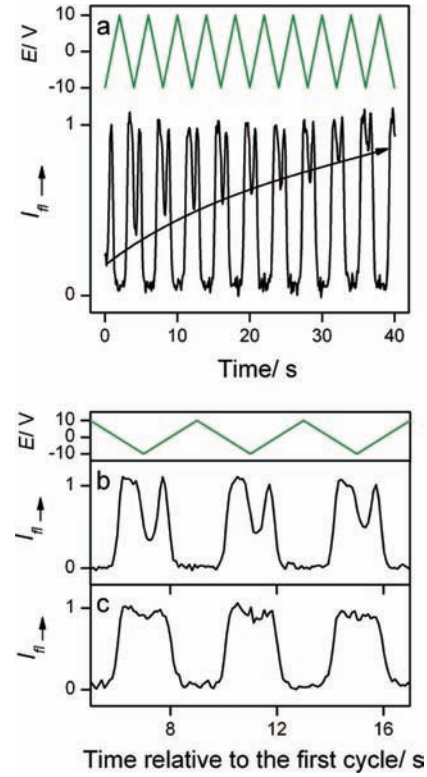

Figure 8. (a) Initial F−V cycles for an ensemble average of 150 normalized fluorescence intensity transients of single MEH-PPV molecules in a type A device with the applied bias shown (green curve). The single MEH-PPV chains were not interrogated previous to the shown run. The arrow shows the decreasing trend of negative bias quenching for the first 10 cycles. (b, c) Initial ensemble average of 50 normalized fluorescence intensity transients of single MEH-PPV molecules in a type A device with (b) 10^{-7} and (c) 5 Torr O_2.

are shown in Figure 7e−h. The red histograms, representing discharging, clearly shift to higher bias when the excitation light intensity decreases. We assign this effect to a shift in the steady-state charge density in MEH-PPV as a function of excitation intensity. At higher excitation intensities, a greater hole density is produced at steady state for the same bias (same CBP hole density). As the light excitation intensity is increased, it is possible to achieve charging at lower biases, i.e., where the CBP hole density is relatively low. Presumably, the $V_{1/2}$ value for the highest excitation intensity of 84 W/cm^2 corresponds to a bias near the threshold of charging the CBP layer, which is about −2 V. Below this bias, no quenching is observed at the relatively high laser powers and very slow scan rates which suggests that below −2 V the CBP has an insignificantly low hole density.

The nearly 100% quenching of the single molecules should be contrasted with the FV-SMS studies of MEH-PPV nanoparticles (~25 nm in radius) which show ~50% quenching depths at comparable excitation rates.[9] In the latter case, the charge density at steady state was assumed to be limited by electrostatic repulsion and screening effects, perhaps involving screening of the CBP/MEH-PPV interface by holes located at the MEH-PPV/insulator interface. For the single-polymer chains described herein (which are considerably smaller than the NP) the effect of excitation seems to dominate the charging process and nearly complete quenching can be achieved. Hole-induced fluorescence quenching in conjugated polymer nanoparticles and single molecules has been previously studied in electrochemical hole-injecting cells.[33,34] In the electrochemical case, the presence of solvent and ions facilitates charge stabilization thus the driving force for hole injection can be made sufficiently high to inject enough holes into the nanoparticles to fully quench their fluorescence.

The presence of single-peak distributions in the charging and discharging histograms and the observed coalescence of the charging and discharging peaks at high laser power strongly suggest that the various molecules in the ensemble have similar charging and discharging kinetics. One contribution to the widths of the $V_{1/2}$ peaks is that the excitation intensity changes as a function of position due to the Gaussian profile of the excitation spot. Preliminary studies with a flat excitation intensity profile reveal a considerably narrower $V_{1/2}$ histogram than shown in the right-hand-side column of Figure 7. This indicates that at least a portion of the apparent broadening of the histogram is due to different rates of hole injection as a result of different excitation intensities for the various particles.

Slow Evolution of F−V SMS Data during Early Bias Cycles. As described above, the ensemble averaged F−V vs. time curves within a bias cycle reveal a time evolution during the first several cycles that then reaches a steady-state dependence on bias that continues indefinitely. Figure 8a reveals that there are in fact two dips (or valleys) during each bias modulation cycle. This is shown in expanded form in Figure 8b. This dip in the fluorescence intensity that occurs for the negative portion of the bias cycle is assigned above to triplet-induced quenching of singlet excitons. This assignment was based on double (light and bias) modulation experiments that have been described previously[9] and also on the observation that when oxygen is added to the sample environment, the dip in the negative bias portion of the cycle disappears, as shown in Figure 8c and in the synchronously averaged data in Figure 5.

On the basis of this assignment, it is interesting that the amount of triplet quenching during negative bias is greatest in the first cycle, decreases gradually for the first 10−15 cycles, and then reaches a steady state amount that persists indefinitely (e.g., 1000 cycles). We speculate that this effect reflects a slow

cycle-to-cycle evolution of the coupling (and energetics) for hole transfer from the CBP layer to the polymer chain. Both effects apparently become more favorable at longer times, leading to more effective triplet quenching. Interestingly, this slow evolution of the triplet quenching is absent when hole transfer is absent, i.e., due to a limited bias range or no optical excitation. Furthermore, it is primarily a single polymer chain effect, not an evolution of the entire device or CBP layer. We speculate that it may be due to a gradual evolution of the conformation of the polymer chain resulting from the charge injection process that occurs during each bias cycle. More research will be necessary to test this hypothesis independently.

4. Conclusions

FV-SMS has been used to explore the kinetics of charging of single MEH-PPV molecules in more detail than previously described, revealing new insights on the molecular level details of the LIHT process. Charge injection kinetics into MEH-PPV as a function of bias scan rate, excitation intensity, and atmosphere were investigated. Charging kinetics were found to be relatively uniform for each single molecule with little molecule-to-molecule variation. The necessity for good electrical contact between the single molecules and the CBP HTL layer to achieve injection was determined through the use of a dielectric blocking layer. In this work, we show that charge injection on the single molecule scale is a complex phenomenon.

Acknowledgment. The authors gratefully acknowledge the Department of Energy, Basic Energy Sciences, the National Science Foundation, the Welch Foundation, and the Air Force Office of Scientific Research for support of this research. Leonid Fradkin acknowledges the Marie Curie Outgoing International Fellowship.

References and Notes

(1) Friend, R. H.; Gymer, R. W.; Holmes, A. B.; Burroughes, J. H.; Marks, R. N.; Taliani, C.; Bradley, D. D. C.; Dos Santos, D. A.; Bredas, J. L.; Logdlund, M.; Salaneck, W. R. *Nature (London)* **1999**, *397*, 121.

(2) Seeley, A. J. A. B.; Friend, R. H.; Kim, J.-S.; Burroughes, J. H. *J. Appl. Phys.* **2004**, *96*, 7643.

(3) Zhang, J. Z. *J. Phys. Chem. B* **2000**, *104*, 7239.

(4) Salaneck, W. R.; Stafstroem, S.; Bredas, J. L., Eds. *Conjugated Polymer Surfaces and Interfaces: Electronic and Chemical Structure of Interfaces for Polymer Light Emitting Devices*; Cambridge University Press: New York, 1996.

(5) Zhu, X. Y. *J. Phys. Chem. B* **2004**, *108*, 8778.

(6) Cahen, D.; Kahn, A. *Adv. Mater.* **2003**, *15*, 271.

(7) Halls, J. J. M.; Cornil, J.; dos Santos, D. A.; Silbey, R.; Hwang, D. H.; Holmes, A. B.; Bredas, J. L.; Friend, R. H. *Phys. Rev. B: Condens. Matter Mater. Phys.* **1999**, *60*, 5721.

(8) Fahlman, M.; Crispin, A.; Crispin, X.; Henze, S. K. M.; de Jong, M. P.; Osikowicz, W.; Tengstedt, C.; Salaneck, W. R. *J. Phys.: Condens. Matter* **2007**, *19*, XXX.

(9) Palacios, R. E.; Lee, K. J.; Rival, A.; Adachi, T.; Bolinger, J. C.; Fradkin, L.; Barbara, P. F. *Chem. Phys.* In press.

(10) Bolinger, J. C.; Fradkin, L.; Lee, K.-J.; Palacios, R. E.; Barbara, P. F. *Proc. Natl. Acad. Sci.* In press.

(11) Bolinger, J. C.; Lee, K. J.; Palacios, R. E.; Barbara, P. F. *J. Phys. Chem. C* **2008**, *112*, 18608.

(12) Guo, T. F.; Yang, F. S.; Tsai, Z. J.; Wen, T. C.; Hsieh, S. N.; Fu, Y. S. *Appl. Phys. Lett.* **2005**, *87*, 013504.

(13) Muller, E. M.; Marohn, J. A. *Adv. Mater. (Weinheim, Germany)* **2005**, *17*, 1410.

(14) Salleo, A.; Street, R. A. *Phys. Rev. B: Condens. Matter Mater. Phys.* **2004**, *70*, 235324/1.

(15) Lang, D. V.; Chi, X.; Siegrist, T.; Sergent, A. M.; Ramirez, A. P. *Phys. Rev. Lett.* **2004**, *93*, 076601/1.

(16) Campbell, A. J.; Bradley, D. D. C.; Antoniadis, H. *Appl. Phys. Lett.* **2001**, *79*, 2133.

(17) Jaquith, M.; Muller, E. M.; Marohn, J. A. *J. Phys. Chem. B* **2007**, *111*, 7711.

(18) Coffey, D. C.; Ginger, D. S. *Nat. Mater.* **2006**, *5*, 735.

(19) Sinha, S.; Monkman, A. P. *J. Appl. Phys.* **2005**, *97*, 114505.

(20) Northrup, J. E.; Chabinyc, M. L. *Phys. Rev. B* **2003**, *68*, 041202.

(21) Kadashchuk, A.; Schmechel, R.; von Seggern, H.; Scherf, U.; Vakhnin, A. *J. Appl. Phys.* **2005**, *98*, 024101/1.

(22) Muller, J. G.; Lemmer, U.; Feldmann, J.; Scherf, U. *Phys. Rev. Lett.* **2002**, *88*, 147401.

(23) Chang, J. B.; Subramanian, V. *Appl. Phys. Lett.* **2006**, *88*, 233513/1.

(24) Gomes, H. L.; Stallinga, P.; Dinelli, F.; Murgia, M.; Biscarini, F.; de Leeuw, D. M.; Muck, T.; Geurts, J.; Molenkamp, L. W.; Wagner, V. *Appl. Phys. Lett.* **2004**, *84*, 3184.

(25) Matters, M.; De Leeuw, D. M.; Herwig, P. T.; Brown, A. R. *Synth. Met.* **1999**, *102*, 998.

(26) Salleo, A.; Street, R. A. *J. Appl. Phys.* **2003**, *94*, 471.

(27) Li, L.; Ruzgas, T.; Gaigalas, A. K. *Langmuir* **1999**, *15*, 6358.

(28) Azoulay, J.; Debarre, A.; Richard, A.; Tchenio, P. *Europhys. Lett.* **2000**, *51*, 374.

(29) Barbara, P. F.; Meyer, T. J.; Ratner, M. A. *J. Phys. Chem.* **1996**, *100*, 13148.

(30) Meli, L.; Li, Y.; Lim, K. T.; Johnston, K. P.; Green, P. F. *Macromolecules* **2007**, *40*, 6713.

(31) Gesquiere, A. J.; Lee, Y. J.; Yu, J.; Barbara, P. F. *J. Phys. Chem. B* **2005**, *109*, 12366.

(32) Yu, J.; Lammi, R.; Gesquiere, A. J.; Barbara, P. F. *J. Phys. Chem. B* **2005**, *109*, 10025.

JP900562W